No-slip and Free-slip divergence-free wavelets in three and higher dimension for the simulation of incompressible viscous flows

Souleymane Kadri, Valérie Perrier

No-slip and Free-slip divergence-free wavelets in three and higher dimension for the simulation of incompressible viscous flows

Souleymane Kadri Harouna and Valérie Perrier

Abstract This work concerns divergence-free wavelet based methods for the numerical resolution of Navier-Stokes equations. It generalizes to higher dimension the approach of [23] that reformulates the projection method using the Helmholtz-Hodge decomposition in wavelet domain. The solution is searched in a finite dimensional free-slip divergence-free wavelet space, with time-dependent wavelet coefficients. We prove and verify the convergence of a first-order time numerical scheme for the Helmholtz-Hodge based projection method. Numerical simulations on the 3D Lid driven cavity flow show the accuracy and efficiency of the method.

1 Introduction

The numerical resolution of the time dependent Navier-Stokes equations for an incompressible viscous fluid still remains a complex problem. The direct numerical simulation where all the flows eddies are simulated is very costly in terms of computational time and memory storage ressources. One reason of such a difficulty is that, commonly, the velocity field and the pressure are coupled in the numerical discretization due to the incompressibility constraint of the velocity field [17, 35]. Moreover, the numerical methods for the resolution of mixed problems (Stokes problem) require an inf-sup condition to be satisfied for the velocity and pressure discretization spaces [17, 36]. In practice, it is difficult to manage both discretizations to obtain this inf-sup condition. Thus, the conditional number of the arising system is very high, which increases the numerical cost of the global method.

Souleymane Kadri Harouna
Laboratoire de Mathématiques Image et Applications, Avenue Michel Crépeau,17042 La Rochelle cedex 1 France, e-mail: souleymane.kadri_harouna@univ-lr.fr

Valérie Perrier
Univ. Grenoble Alpes, CNRS, Grenoble INP, LJK, 38000 Grenoble, France, e-mail: Valerie.Perrier@univ-grenoble-alpes.fr

By their property of data sparse representation, wavelet based methods have been introduced in the numerical resolution of the Stokes problem to get robust and effective numerical schemes, with lower data storage. Principally, wavelet bases linked by differentiation and integration allows to stabilize the spatial discretizations, and get the inf-sup condition [2, 32], another interest lies in the ability to provide adaptive strategies to reduce the algorithm complexity [3, 6, 7, 14, 15, 16, 31, 32, 36].

The projection method initialized by Chorin and Temam [4, 34] is an approach that avoids the difficulties of the Stokes problem: it is based on a time splitting method that uncouples the computation of the velocity field from the pressure. An intermediate velocity is computed and then, this predicted velocity is projected onto the space of divergence-free vector fields. The simplicity of the method lies in the fact that the prediction and the correction steps are elliptic problems, namely Poisson equations. However, the projection method introduces an additional numerical splitting error, which must be at worst of the same order as the time discretization error. In addition, the corrected velocity field does not satisfy the desired boundary condition, and the projection step imposes an artificial boundary condition on the pressure [12].

A reformulation of the projection method was proposed in [23] consisting in a change of variable like in the Gauge method [27, 38]. The main idea of [23] is to replace the classical correction step by a Helmholtz-Hodge decomposition of the intermediate predicted velocity field, using a divergence-free wavelet basis. This allows to directly encode the boundary conditions into the divergence-free wavelet basis and avoids the use of non-physical boundary conditions for the pressure. The numerical complexity of the divergence-free wavelet based Helmholtz-Hodge decomposition does not exceed than of the resolution of a Poisson equation, see [21].

The achievements of the present paper is to propose an extension of [23] to the three-dimensional case, to provide a convergence result and 3D numerical simulations. First we describe a recent construction of divergence-free wavelets, more easy to handle, satisfying no-slip and free-slip boundary condition on the hypercube in dimension 3, borrowed from [24]. Then following the approach of [23] for the 2D case, we use these divergence-free wavelets to design a numerical method for the resolution of Navier-Stokes equations in 3D. As done for the 2D (linear) Stokes equations in [23], we study here the convergence of the method for the (nonlinear) 3D Navier-Stokes equations, using a first-order time-discretization scheme. Then, a standard error analysis allows us to prove the convergence of the numerical scheme, under a CFL type condition. Numerical experiments conducted on benchmark flows confirm these theoretical results.

This paper is organized as follows. Section 2 summarizes the principle of the construction of divergence-free wavelet bases. We recall in Section 2.1 the construction of the one-dimensional biorthogonal multiresolution analyses linked by differentiation and integration that we used to construct divergence-free wavelets

satisfying physical boundary conditions in Section 2.2. Section 3 present the numerical method, and we investigate the convergence of the time-discretization scheme in the energy norm. Section 4, describes our fully discrete scheme and presents numerical simulation results on benchmark flow, particularly the 3D lid driven cavity flow.

2 Free-slip divergence-free wavelet bases on $[0,1]^d$

Since the seminal works of Lemarié-Rieusset and collaborators [20, 26], several constructions of divergence-free (and curl-free) wavelet bases on $[0,1]^d$ have been provided in the literature [10, 22, 32, 33, 36, 37]. The free-slip boundary condition case was treated by several methods in [22, 32, 33]. In this section, we follow the construction principle of [22, 24], which we extend to general dimension. We begin with our construction of biorthogonal multiresolution analyses of $L^2(0,1)$ linked by differentiation and integration.

2.1 Multiresolution analyses linked by differentiation and integration

Divergence-free wavelet constructions on the hypercube require the use of multiresolution analyses on the interval linked by differentiation and integration [20, 22, 32]. Specifically, we would like to have at hand two biorthogonal multiresolution analyses of $L^2(0,1)$, denoted by $(V_j^1, \tilde{V}_j^1)$ and $(V_j^0, \tilde{V}_j^0)$ satisfying:

$$\frac{d}{dx} V_j^1 = V_j^0. \tag{1}$$

The construction of the biorthogonal spaces $\tilde{V}_j^1$ and $\tilde{V}_j^0$ is of the utmost importance. A suitable choice would provide the commutation of the multi-scale projectors with the derivation operator. Such a choice was suggested in [20, 22]:

$$\tilde{V}_j^0 = \left\{ \int_0^x f(t)dt \ : \ f \in \tilde{V}_j^1 \right\} \cap H_0^1(0,1)^1 \Rightarrow \frac{d}{dx} \tilde{V}_j^0 \subset V_j^0. \tag{2}$$

In this case, we have:

$$\frac{d}{dx} \circ \mathcal{P}_j^1 = \mathcal{P}_j^0 \circ \frac{d}{dx}, \tag{3}$$

[1] For $m \in \mathbb{N}^*$, $H^m(0,1)$ denotes the Sobolev space of order m:

- $H^m(0,1) = \{u \in L^2(0,1) \ : \ u' \in L^2(0,1), \ldots, u^{(m)} \in L^2(0,1)\}$.
- $H_0^m(0,1) = \{u \in H^m(0,1) \ : \ u(0) = u(1) = 0, \ldots, u^{(m-1)}(0) = u^{(m-1)}(1) = 0\}$.
- $H^s(0,1) = \{u \in H^m(0,1) \ : \ m < s < m+1$ and $\int_0^1 \int_0^1 \frac{|u^{(m)}(x) - u^{(m)}(y)|^2}{|x-y|^{2(s-m)+1}} dxdy < +\infty\}$.

where $\mathcal{P}_j^1$ is biorthogonal projector onto V_j^1 and $\mathcal{P}_j^0$ the biorthogonal projector onto V_j^0. A significant property of such a construction is that the spaces $\tilde{V}_j^0$ provide a multiresolution analysis for $H_0^1(0,1)$ (and not for $L^2(0,1)$). However, the edge wavelets of [22] do not satisfy a diagonal differentiation relation. A remedy to this was proposed in [32, 33], where the commutation property of the multi-scale projectors and the derivation operator is lost. Another construction proposed in [24] consists in setting:

$$\frac{d}{dx}\tilde{V}_j^0 = \tilde{V}_j^d, \tag{4}$$

where $\tilde{V}_j^d$ is the biorthogonal space of the space satisfying homogeneous Dirichlet boundary conditions $V_j^d = V_j^1 \cap H_0^1(0,1)$, and $\tilde{V}_j^d \not\subset H_0^1(0,1)$. This choice preserves the commutation property and leads to a diagonal differentiation relation for the wavelet bases even for edge wavelets.

The constructions of [20, 22] are based on multiresolution analyses of $L^2(0,1)$ reproducing polynomials at boundaries [5, 28, 29]. Each space is spanned by a scaling functions basis:

$$V_j^1 = \text{span}\{\varphi_{j,k}^1 \ ; \ 0 \le k \le N_j - 1\} \ \text{ and } \ \tilde{V}_j^1 = \text{span}\{\tilde{\varphi}_{j,k}^1 \ ; \ 0 \le k \le N_j - 1\},$$

and

$$V_j^0 = \text{span}\{\varphi_{j,k}^0 \ ; \ 0 \le k \le N_j - 2\} \ \text{ and } \ \tilde{V}_j^0 = \text{span}\{\tilde{\varphi}_{j,k}^0 \ ; \ 0 \le k \le N_j - 2\},$$

with dimension parameter $N_j = 2^j + c$, for $c \in \mathbb{Z}$. For $\varepsilon = 0, 1$, the scaling functions $\varphi_{j,k}^\varepsilon$ can be written as $\varphi_{j,k}^\varepsilon = 2^{j/2}\varphi^\varepsilon(2^j x - k)$ inside the interval $[0,1]$, where φ^ε is a compactly supported scaling function on $\mathbb{R}$, but this is no more true near the boundaries 0 and 1 (idem for $\tilde{\varphi}_{j,k}^\varepsilon$). In practice, the scale index j must be greater than some index j_{min}, to avoid boundary effects [29]. The biorthogonality between bases writes:

$$\langle \varphi_{j,k}^\varepsilon, \tilde{\varphi}_{j,k'}^\varepsilon \rangle = \delta_{k,k'}.$$

The advantage of using multiresolution analyses reproducing polynomials at boundaries is that homogeneous boundary conditions can be easily incorporated. It suffices to remove the scaling functions that do not satisfy the desired condition at edges 0 and 1, prior to biorthogonalization [28, 29]. This writes:

$$V_j^d = V_j^1 \cap H_0^1(0,1) = \text{span}\{\varphi_{j,k}^1 \ ; \ 1 \le k \le N_j - 2\}, \tag{5}$$

and

$$V_j^{dd} = V_j^1 \cap H_0^2(0,1) = \text{span}\{\varphi_{j,k}^1 \ ; \ 2 \le k \le N_j - 3\}. \tag{6}$$

Again, for the construction of the biorthogonal spaces $\tilde{V}_j^d$ and $\tilde{V}_j^{dd}$, we proceed similarly by removing edge scaling functions, to ensure the equality of dimensions and this leads to $(V_j^d, \tilde{V}_j^d)$ and $(V_j^{dd}, \tilde{V}_j^{dd})$, biorthogonal multiresolution analyses of

$H_0^1(0,1)$ and $H_0^2(0,1)$ respectively [28]. Notice that the spaces $\tilde{V}_j^d$ and $\tilde{V}_j^{dd}$ provide multiresolution analyses of $L^2(0,1)$, see [24, 28].

Following the standard constructions [5, 18], the wavelets in the biorthogonal multiresolution analysis $(V_j^1, \tilde{V}_j^1)$ are defined as the bases of the biorthogonal spaces:

$$W_j^1 = V_{j+1}^1 \cap (\tilde{V}_j^1)^\perp \text{ and } \tilde{W}_j^1 = \tilde{V}_{j+1}^1 \cap (V_j^1)^\perp.$$

These spaces are finite dimensional [5]:

$$W_j^1 = \text{span}\{\psi_{j,k}^1 \ ; \ 0 \le k \le 2^j - 1\} \text{ and } \tilde{W}_j^1 = \text{span}\{\tilde{\psi}_{j,k}^1 \ ; \ 0 \le k \le 2^j - 1\},$$

with:

$$\langle \psi_{j,k}^1, \tilde{\psi}_{j',k'}^1 \rangle = \delta_{j,j'}\delta_{k,k'} \text{ and } \langle \psi_{j,k}^1, \tilde{\varphi}_{j',k'}^1 \rangle = 0.$$

Then working in $H_0^1(0,1)$, a first possibility is to construct the wavelet spaces as in [28, 29]:

$$W_j^d = V_{j+1}^d \cap (\tilde{V}_j^d)^\perp \text{ and } \tilde{W}_j^d = \tilde{V}_{j+1}^d \cap (V_j^d)^\perp.$$

This possibility was at the origin of the construction [22]. But unfortunately the diagonal relation with the derivation is lost for edge wavelets. To overcome this difficulty another approach was proposed by [24] and consists in first using a standard construction for the wavelet bases of $W_j^0 = V_{j+1}^0 \cap (\tilde{V}_j^0)^\perp$ and $\tilde{W}_j^0 = \tilde{V}_{j+1}^0 \cap (V_j^0)^\perp$[5, 18, 28, 29], denoted by $\{\psi_{j,k}^0\}_{j \ge j_{min}}$ and $\{\tilde{\psi}_{j,k}^0\}_{j \ge j_{min}}$. In a second step, the wavelets of W_j^d and $\tilde{W}_j^d$ are defined by:

$$\psi_{j,k}^d = 2^j \int_0^x \psi_{j,k}^0 \qquad \text{and} \qquad 2^{-j}(\tilde{\psi}_{j,k}^0)' = -\tilde{\psi}_{j,k}^d. \tag{7}$$

As remarked before, this definition is different from this of [20, 22] where the wavelets $\psi_{j,k}^d$ and $\tilde{\psi}_{j,k}^d$ were defined first and second one set: $\psi_{j,k}^0 = 2^{-j}(\psi_{j,k}^d)'$ and $\tilde{\psi}_{j,k}^d = -2^j \int_0^x \tilde{\psi}_{j,k}^d$.
Now, due to the vanishing moments of $\psi_{j,k}^0$, it is easy to see that definition (7) implies $\psi_{j,k}^d \in H_0^1(0,1)$ and for any $j > j_{min}$:

$$V_j^d = V_{j_{min}}^d \oplus W_{j_{min}}^d \oplus \cdots \oplus W_{j-1}^d. \tag{8}$$

Decomposition (8) is stable in $H_0^1(0,1)$, *i.e.* the system $\{\psi_{j,k}^d\}_{j \ge j_{min}} \cup \{\varphi_{j_{min},k}^d\}$ is a Riesz basis for $H_0^1(0,1)$, see [24].

For each basis, a fast wavelet transform algorithm exists with a linear complexity and the approximation order of each multiresolution analysis space is linked to the number of vanishing moments of its biorthogonal wavelets [5, 22, 28, 29]. Precisely, if φ^1 allows to reproduce polynomials up to degree $r-1$ in V_j^1, thus the biorthogonal

wavelet $\tilde{\psi}^1$ has r vanishing moments :

$$\int_{-\infty}^{+\infty} x^\ell \tilde{\psi}^1(x)dx = 0 \ \text{ for } \ 0 \leq \ell \leq r-1.$$

Then, due to the differentiation and integration relations (1) and (4), the wavelet $\tilde{\psi}^0$ has $(r-1)$ vanishing moments and ψ^0 has $(\tilde{r}+1)$ vanishing moments.

2.2 Free-slip and no-slip divergence-free wavelet construction

In this section, we recall the construction of free-slip divergence-free wavelets on the hypercube $[0,1]^3$ as proposed in [21, 24]. Then we outline the construction of no-slip divergence-free wavelets. Next section will sketch the general form of no-slip divergence-free wavelets to higher space dimension $d > 3$.

The divergence-free function space with free-slip boundary conditions is:

$$\mathcal{H}_{div}(\Omega) = \{\boldsymbol{u} \in (L^2(\Omega))^3 : \ \nabla \cdot \boldsymbol{u} = 0 \text{ and } \boldsymbol{u} \cdot \boldsymbol{n}|_{\partial\Omega} = 0\}, \tag{9}$$

where $\Omega = [0,1]^3$ and $\boldsymbol{n}$ denotes the unit outward normal to boundary $\partial\Omega$. Then, following [21] there are three kind of divergence-free scaling functions in $\mathcal{H}_{div}(\Omega)$ defined by:

$$\Phi^{div,1}_{j,\boldsymbol{k}} := \mathbf{curl} \begin{bmatrix} 0 \\ 0 \\ \varphi^d_{j,k_1} \otimes \varphi^d_{j,k_2} \otimes \varphi^0_{j,k_3} \end{bmatrix} = \begin{bmatrix} \varphi^d_{j,k_1} \otimes (\varphi^d_{j,k_2})' \otimes \varphi^0_{j,k_3} \\ -(\varphi^d_{j,k_1})' \otimes \varphi^d_{j,k_2} \otimes \varphi^0_{j,k_3} \\ 0 \end{bmatrix}, \tag{10}$$

$$\Phi^{div,2}_{j,\boldsymbol{k}} := \mathbf{curl} \begin{bmatrix} \varphi^0_{j,k_1} \otimes \varphi^d_{j,k_2} \otimes \varphi^d_{j,k_3} \\ 0 \\ 0 \end{bmatrix} = \begin{bmatrix} 0 \\ \varphi^0_{j,k_1} \otimes \varphi^d_{j,k_2} \otimes (\varphi^d_{j,k_3})' \\ -\varphi^0_{j,k_1} \otimes (\varphi^d_{j,k_2})' \otimes \varphi^d_{j,k_3} \end{bmatrix}, \tag{11}$$

$$\Phi^{div,3}_{j,\boldsymbol{k}} := \mathbf{curl} \begin{bmatrix} 0 \\ \varphi^d_{j,k_1} \otimes \varphi^0_{j,k_2} \otimes \varphi^d_{j,k_3} \\ 0 \end{bmatrix} = \begin{bmatrix} -\varphi^d_{j,k_1} \otimes \varphi^0_{j,k_2} \otimes (\varphi^d_{j,k_3})' \\ 0 \\ (\varphi^d_{j,k_1})' \otimes \varphi^0_{j,k_2} \otimes \varphi^d_{j,k_3} \end{bmatrix}. \tag{12}$$

By construction these scaling functions are in $\mathcal{H}_{div}(\Omega)$ and the space $\mathbf{V}^{div}_j$ that they spanned is included into the multiresolution analysis of $(L^2(\Omega))^3$ given by:

$$\mathbf{V}^{div}_j \subset \mathbf{V}^d_j = \left(V^d_j \otimes V^0_j \otimes V^0_j\right) \times \left(V^0_j \otimes V^d_j \otimes V^0_j\right) \times \left(V^0_j \otimes V^0_j \otimes V^d_j\right). \tag{13}$$

Moreover, let $\mathbf{P}_j$ be the biorthogonal multiscale projector onto $\mathbf{V}^d_j$:

$$\mathbf{P}_j = \left(\mathcal{P}_j^d \otimes \mathcal{P}_j^0 \otimes \mathcal{P}_j^0\right) \times \left(\mathcal{P}_j^0 \otimes \mathcal{P}_j^d \otimes \mathcal{P}_j^0\right) \times \left(\mathcal{P}_j^0 \otimes \mathcal{P}_j^0 \otimes \mathcal{P}_j^d\right),$$

and

$$\mathbf{P}_j^0 = \mathcal{P}_j^0 \otimes \mathcal{P}_j^0 \otimes \mathcal{P}_j^0,$$

the biorthogonal multiscale projector onto $\mathbf{V}_j^0 = V_j^0 \otimes V_j^0 \otimes V_j^0$. Due to the commutation property (3), we have:

$$\forall\ \boldsymbol{u} \in \mathcal{H}_{div}(\Omega),\ \nabla \cdot \mathbf{P}_j(\boldsymbol{u}) = \mathbf{P}_j^0(\nabla \cdot \boldsymbol{u}) = 0$$

In terms of spaces this rewrites $\mathbf{P}_j(\mathcal{H}_{div}(\Omega)) = \mathbf{V}_j \cap \mathcal{H}_{div}(\Omega)$. Therefore, the spaces $\mathbf{V}_j^{div} = \mathbf{V}_j \cap \mathcal{H}_{div}(\Omega)$ provide a multiresolution analysis of $\mathcal{H}_{div}(\Omega)$ and a basis of $\mathbf{V}_j^{div}$ is generated by choosing two of the scaling function generators listed above [24]. Beside, from each scaling function generator, one can construct 7 types of anisotropic divergence-free wavelets [10, 24, 26]. We denote by $\{\Psi_{\boldsymbol{j},\boldsymbol{k}}^{div,1}, \Psi_{\boldsymbol{j},\boldsymbol{k}}^{div,2}\}$ the wavelets corresponding to $\{\Phi_{j,\boldsymbol{k}}^{div,1}, \Phi_{j,\boldsymbol{k}}^{div,2}\}$ and $\mathbf{W}_j^{div}$ the space they span:

$$\mathbf{W}_{\boldsymbol{j}}^{div} = span\left\{\Psi_{\boldsymbol{j},\boldsymbol{k}}^{div,1}, \Psi_{\boldsymbol{j},\boldsymbol{k}}^{div,2}\right\}_{j_{min} \le |\boldsymbol{j}| \le j-1}, \tag{14}$$

where the index $\boldsymbol{k} = (k_1, k_2, k_3)$ varies depending on the corresponding function: if one coordinate of $\boldsymbol{k}$ corresponds to a wavelet $\psi_{j,k}^d$ or $\psi_{j,k}^0$, we take $1 \le k \le 2^j$; if it corresponds to a scaling function $\varphi_{j,k}^d$, we take $1 \le k \le N_j - 2$; if it corresponds to a scaling function $\varphi_{j,k}^0$, we take $0 \le k \le N_j - 2$. In the sequel, we will use this convention for all the summation over the index $\boldsymbol{k}$.

According to (14), the anisotropic multiscale decomposition of $\mathbf{V}_j^{div}$ corresponds to:

$$\mathbf{V}_j^{div} = \mathbf{V}_{j_{min}}^{div} \bigoplus_{j_{min} \le |\boldsymbol{j}| \le j-1} \mathbf{W}_{\boldsymbol{j}}^{div}, \tag{15}$$

and since the spaces $\mathbf{V}_j^{div}$ provide a multiresolution analysis of $\mathcal{H}_{div}(\Omega)$, decomposition (15) is stable for this space. Specifically, we have the following proposition [24]:

Proposition 1 *For every function $\boldsymbol{u} \in \mathcal{H}_{div}(\Omega)$, there are coefficients $c_{\boldsymbol{k}}^{div,\epsilon}$ and $d_{\boldsymbol{j},\boldsymbol{k}}^{div,\epsilon}$ such that:*

$$\boldsymbol{u} = \sum_{\epsilon=1}^{2}\left(\sum_{\boldsymbol{k}} c_{\boldsymbol{k}}^{div,\epsilon}\Phi_{j_{min},\boldsymbol{k}}^{div,\epsilon} + \sum_{|\boldsymbol{j}| \ge j_{min}}\sum_{\boldsymbol{k}} d_{\boldsymbol{j},\boldsymbol{k}}^{div,\epsilon}\Psi_{\boldsymbol{j},\boldsymbol{k}}^{div,\epsilon}\right), \tag{16}$$

and for two positive constants C_1 and C_2 independent of $\boldsymbol{u}$, we have:

$$C_1\|\boldsymbol{u}\|_{L^2} \leq \left(\sum_{\epsilon=1}^{2}\sum_{\boldsymbol{k}}|c_{\boldsymbol{k}}^{div,\epsilon}|^2 + \sum_{\epsilon=1}^{2}\sum_{|\boldsymbol{j}|\geq j_{min}}\sum_{\boldsymbol{k}}|d_{\boldsymbol{j},\boldsymbol{k}}^{div,\epsilon}|^2\right)^{1/2} \leq C_2\|\boldsymbol{u}\|_{L^2}. \quad (17)$$

Proposition 1 is immediate using Lemma 2 borrowed from [20, 26] and reported in the Appendix Section. Precisely, the constructed divergence-free wavelets and their duals satisfy the hypothesis of this lemma, see [24].

The approximation error provided by the divergence-free wavelet basis is linked to the approximation order of the spaces V_j^1. If the spaces V_j^1 contain polynomials up to degree $r-1$, then V_j^0 contain polynomials up degree $r-2$ and for all $\boldsymbol{u} \in (H^s(\Omega))^3 \cap \mathcal{H}_{div}(\Omega)$ with $0 \leq s \leq r-1$, the following Jackson type estimation holds:

$$\|\boldsymbol{u} - \mathbb{P}_j^{div}(\boldsymbol{u})\|_{L^2} \leq C2^{-js}\|\boldsymbol{u}\|_{H^s}, \quad (18)$$

where $\mathbb{P}_j^{div}$ is the biorthogonal multiscale projector onto $\mathbf{V}_j^{div}$:

$$\mathbb{P}_j^{div}(\boldsymbol{u}) = \sum_{\epsilon=1}^{2}\left(\sum_{\boldsymbol{k}} c_{\boldsymbol{k}}^{div,\epsilon}\Phi_{j_{min},\boldsymbol{k}}^{div,\epsilon} + \sum_{j_{min}\leq|\boldsymbol{j}|\leq j-1}\sum_{\boldsymbol{k}} d_{\boldsymbol{j},\boldsymbol{k}}^{div,\epsilon}\Psi_{\boldsymbol{j},\boldsymbol{k}}^{div,\epsilon}\right). \quad (19)$$

For homogeneous Dirichlet boundary conditions, the divergence-free function space is slightly different, and will be denoted by:

$$\mathcal{H}_{div,0}(\Omega) = \left\{\boldsymbol{u} \in (H_0^1(\Omega))^3 : \nabla\cdot\boldsymbol{u} = 0\right\} = (H_0^1(\Omega))^3 \cap \mathcal{H}_{div}(\Omega).$$

The space $\mathcal{H}_{div,0}(\Omega)$ is a closed subspace of $(H_0^1(\Omega))^3$, then we have the following decomposition:

$$(H_0^1(\Omega))^3 = \mathcal{H}_{div,0}(\Omega) \oplus \mathcal{H}_{div,0}(\Omega)^{\perp},$$

which is an orthogonal decomposition with respect to the inner product of $(H_0^1(\Omega))^3$: $(\boldsymbol{u},\boldsymbol{v})_{(H_0^1(\Omega))^2} = (\nabla\boldsymbol{u},\nabla\boldsymbol{v})_{(L^2(\Omega))^3}$, see [17] for details.

Since $\mathcal{H}_{div,0}(\Omega) \subset \mathcal{H}_{div}(\Omega)$, a multiresolution analysis of $\mathcal{H}_{div,0}(\Omega)$ is then provided by the spaces:

$$\mathbf{V}_j^{div,0} = \mathbf{V}_j^{dd} \cap \mathcal{H}_{div,0}(\Omega),$$

where

$$\mathbf{V}_j^{dd} = \left(V_j^{dd}\otimes V_j^{00}\otimes V_j^{00}\right) \times \left(V_j^{00}\otimes V_j^{dd}\otimes V_j^{00}\right) \times \left(V_j^{00}\otimes V_j^{00}\otimes V_j^{dd}\right), \quad (20)$$

and $V_j^{00} = V_j^0 \cap H_0^1(0,1)$. A scaling function basis of $\mathbf{V}_j^{div,0}$ is then given by:

$$\Phi^{div,0,1}_{j,\boldsymbol{k}} := \mathbf{curl} \begin{bmatrix} 0 \\ 0 \\ \varphi^{dd}_{j,k_1} \otimes \varphi^{dd}_{j,k_2} \otimes \varphi^{00}_{j,k_3} \end{bmatrix} = \begin{bmatrix} \varphi^{dd}_{j,k_1} \otimes (\varphi^{dd}_{j,k_2})' \otimes \varphi^{00}_{j,k_3} \\ -(\varphi^{dd}_{j,k_1})' \otimes \varphi^{dd}_{j,k_2} \otimes \varphi^{00}_{j,k_3} \\ 0 \end{bmatrix}, \tag{21}$$

$$\Phi^{div,0,2}_{j,\boldsymbol{k}} := \mathbf{curl} \begin{bmatrix} \varphi^{00}_{j,k_1} \otimes \varphi^{dd}_{j,k_2} \otimes \varphi^{dd}_{j,k_3} \\ 0 \\ 0 \end{bmatrix} = \begin{bmatrix} 0 \\ \varphi^{00}_{j,k_1} \otimes \varphi^{dd}_{j,k_2} \otimes (\varphi^{dd}_{j,k_3})' \\ -\varphi^{00}_{j,k_1} \otimes (\varphi^{dd}_{j,k_2})' \otimes \varphi^{dd}_{j,k_3} \end{bmatrix}, \tag{22}$$

$$\Phi^{div,0,3}_{j,\boldsymbol{k}} := \mathbf{curl} \begin{bmatrix} 0 \\ \varphi^{dd}_{j,k_1} \otimes \varphi^{00}_{j,k_2} \otimes \varphi^{dd}_{j,k_3} \\ 0 \end{bmatrix} = \begin{bmatrix} -\varphi^{dd}_{j,k_1} \otimes \varphi^{00}_{j,k_2} \otimes (\varphi^{dd}_{j,k_3})' \\ 0 \\ (\varphi^{dd}_{j,k_1})' \otimes \varphi^{00}_{j,k_2} \otimes \varphi^{dd}_{j,k_3} \end{bmatrix}, \tag{23}$$

where $\{\varphi^{00}_{j,k}\}_{1\le k\le N_j-3} = \{\varphi^{0}_{j,k}\}_{1\le k\le N_j-3}$ is the scaling function basis of V^{00}_j [29].

Similarly, to construct no-slip divergence-free wavelets associated to $\mathbf{V}^{div,0}_j$, it suffices to replace the wavelets of W^d_j by those of $W^{dd}_j = V^{dd}_{j+1} \cap (\tilde{V}^{dd}_j)^{\perp}$ in the formula which defines the functions $\{\Psi^{div,\epsilon}_{\boldsymbol{j},\boldsymbol{k}}\}_{\epsilon=1,2,3}$, see [22, 33]. Let now $\mathbb{P}^{div,0}_j$ be the L^2-orthogonal projector from $(H^1_0(\Omega))^3$ onto $\mathbf{V}^{div,0}_j$. Again, for all $\boldsymbol{u} \in (H^s(\Omega))^3$ with $1 \le s \le r-1$, the following Jackson type estimation holds, for some $C > 0$:

$$\|\boldsymbol{u} - \mathbb{P}^{div,0}_j(\boldsymbol{u})\|_{H^1_0} \le C\, 2^{-j(s-1)} \|\boldsymbol{u}\|_{H^s}. \tag{24}$$

2.3 Extension to higher dimension $d > 3$.

The divergence-free wavelet basis construction is not limited to dimension 3 only. Several applications such as image warping [30], optimal transportation [19] or magnetohydrodynamic turbulence [13], involve divergence-free vector fields living in spaces of dimension d greater than 3. This divergence-free contraint for the solution leads in general to solve a Poisson equation difficult to handle. Therefore it would be of great interest to have at hand divergence-free bases that enable to encode such solution.

The construction of previous section extends to larger dimensions $d > 3$ readily. As in [8, 26] we obtain in this case $(d-1)$ types of linear independent divergence-free wavelet functions. For $1 \le i \le d-1$, the general formula of these wavelets is given by:

$$\Psi^{div,i}_{\boldsymbol{j},\boldsymbol{k}} := \begin{bmatrix} 0 \\ \vdots \\ 0 \\ 2^{j_{i+1}}\psi^0_{j_1,k_1} \otimes \cdots \otimes \psi^0_{j_{i-1},k_{i-1}} \otimes \psi^d_{j_i,k_i} \otimes \psi^0_{j_{i+1},k_{i+1}} \otimes \cdots \otimes \psi^0_{j_d,k_d} \\ -2^{j_i}\psi^0_{j_1,k_1} \otimes \cdots \otimes \psi^0_{j_i,k_i} \otimes \psi^d_{j_{i+1},k_{i+1}} \otimes \psi^0_{j_{i+1},k_{i+2}} \otimes \cdots \otimes \psi^0_{j_d,k_d} \\ 0 \\ \vdots \\ 0 \end{bmatrix}, \quad (25)$$

where only the row i and row $i+1$ are not zeros.

Recalling that $(\psi^d_{j_i,k_i})' = 2^{j_i}\psi^0_{j_i,k_i}$, we easily verify that $\nabla \cdot \Psi^{div,i}_{\boldsymbol{j},\boldsymbol{k}} = 0$, and that the $\Psi^{div,i}_{\boldsymbol{j},\boldsymbol{k}}$ satisfy the boundary condition $\Psi^{div,i}_{\boldsymbol{j},\boldsymbol{k}} \cdot \boldsymbol{n} = 0$. The space $\mathbf{W}^{div}_{\boldsymbol{j}}$ spanned by these wavelets is included into the following standard BMRA of $(L^2(\Omega))^d$:

$$\mathbf{V}_j = \mathbf{V}^1_j \times \cdots \times \mathbf{V}^d_j \quad \text{with} \quad \mathbf{V}^i_j = V^{\delta_{1,i}}_j \otimes \cdots \otimes V^{\delta_{d,i}}_j, \ \ 1 \le i \le d, \qquad (26)$$

where $\delta_{i,j}$ denotes the Kronecker symbol. To satisfy the free-slip boundary condition we must replace V^1_j by V^d_j in (26). We also emphasized that, the corresponding spaces $\mathbf{V}^{div}_j = \mathbf{V}_j \cap \mathcal{H}_{div}(\Omega) = \mathbf{P}_j(\mathcal{H}_{div}(\Omega))$ provide a multiresolution analysis of $\mathcal{H}_{div}(\Omega)$. Following a similar approach as for $d = 3$, and taking $(d-1)$ scaling functions, we obtain a divergence-free basis of $\mathbf{V}^{div}_j$.

3 Divergence-free wavelet schemes for the Navier-Stokes equations

The motions of incompressible homogeneous viscous flows, confined in an open domain $\Omega \subset \mathbb{R}^d$ with smooth boundary $\Gamma = \partial\Omega$, are governed by the time-depending Navier-Stokes equations:

$$\begin{cases} \partial_t \boldsymbol{v} - \nu\Delta\boldsymbol{v} + (\boldsymbol{v}\cdot\nabla)\boldsymbol{v} + \nabla p = \boldsymbol{f}, \\ \\ \nabla \cdot \boldsymbol{v} = 0, \end{cases} \qquad (27)$$

where $\boldsymbol{v} \in \mathbb{R}^d$ denotes the velocity vector field, $p \in \mathbb{R}$ is the pressure, $\nu > 0$ is the kinematic viscosity and $\boldsymbol{f}$ the external force. Without loss of generality, we will assume that $\boldsymbol{f} = 0$. System (27) is supplemented by boundary conditions and throughout this section, we will assume the no-slip boundary condition $\boldsymbol{v} = 0$ on Γ. Non-homogeneous Dirichlet boundary condition $\boldsymbol{v} = g$ on Γ will be handled in the numerical experiments.

The objective in this section is to study the numerical approximation of (27) using divergence-free wavelet based methods. These schemes use the divergence-free wavelet Leray projector to decouple the computation of the velocity and the pressure, as in the case of the Fourier spectral method [9, 10, 23], thus they avoid the resolution of a Stokes problem. In this section we propose to investigate the generalization of the method of [23] to the three dimensional Navier-Stokes equations. We begin with the description and the study of the temporal and spatial discretizations.

3.1 Temporal discretization

Let $\delta t > 0$ be a time step. For $0 \leq n \leq N$, we set $t_n = n\delta t$ such that $0 = t_0 < t_1 < \cdots < t_N = T$ is a uniform partition of the computational time interval. We denote by $\boldsymbol{v}^n$ and p^n the approximations of $\boldsymbol{v}(t_n, x)$ and $p(t_n, x)$, where $(\boldsymbol{v}, p)$ is a smooth solution of (27). To compute $(\boldsymbol{v}^n, p^n)$, the approach of [23] consists in replacing the classical correction step of the projection method [4, 34] by a divergence-free wavelet Leray-Hodje projector. Specifically, since $(H_0^1(\Omega))^d = \mathcal{H}_{div,0}(\Omega) \oplus \mathcal{H}_{div,0}(\Omega)^{\perp}$, there exists Φ^{n+1}, a scalar potential in $L^2(\Omega)$ such that:

$$\tilde{\boldsymbol{v}}^{n+1} = \boldsymbol{v}^{n+1} + \nabla\Phi^{n+1}, \quad \text{with} \quad \tilde{\boldsymbol{v}}^{n+1} \in (H_0^1(\Omega))^d. \tag{28}$$

Then, substituting this change of variable in the Navier-Stokes equations (27) and using a projection method time step, with an implicit Euler scheme in time for the diffusion term, we get:

- Prediction step:

$$\begin{cases} \frac{\tilde{\boldsymbol{v}}^{n+1} - \boldsymbol{v}^n}{\delta t} + (\boldsymbol{v}^n \cdot \nabla)\boldsymbol{v}^n = \nu\Delta\tilde{\boldsymbol{v}}^{n+1}, \\ \tilde{\boldsymbol{v}}^{n+1} = 0, \quad \text{on} \quad \partial\Omega. \end{cases} \tag{29}$$

- Correction step:

$$\begin{cases} \boldsymbol{v}^{n+1} = \mathbb{P}^{div,0}(\tilde{\boldsymbol{v}}^{n+1}), \\ \\ p^{n+1} = \frac{1}{\delta t}\Phi^{n+1} - \nu\Delta\Phi^{n+1}. \end{cases} \tag{30}$$

where the correction step of the standard projection method has been modified by introducing $\mathbb{P}^{div,0}$, the L^2-orthogonal projector from $(H_0^1(\Omega))^2$ onto $\mathcal{H}_{div,0}(\Omega)$. Remark that the Navier-Stokes formulation (29) and (30) is no more than a change of variables, whereas the classical projection method is an operator splitting, which implies a loss of precision in time.

The problem defined by (29)-(30) is well posed, in the sense that the numerical solution $\tilde{\boldsymbol{v}}^{n+1}$ exists for given smooth initial data. Indeed, let us define the bilinear form $\boldsymbol{a}(.,.)$:

$$\boldsymbol{a}(\boldsymbol{u},\boldsymbol{v}) = \int_\Omega \boldsymbol{u}\cdot\boldsymbol{v} + \nu\delta t \int_\Omega \nabla\boldsymbol{u} : \nabla\boldsymbol{v},\ \ \forall\ \boldsymbol{u},\boldsymbol{v} \in H_0^1(\Omega)^d, \tag{31}$$

and the linear form L:

$$L(\boldsymbol{v}) = \int_\Omega \boldsymbol{v}^n\cdot\boldsymbol{v} - \delta t \int_\Omega (\boldsymbol{v}^n\cdot\nabla)\boldsymbol{v}^n\cdot\boldsymbol{v}, \forall\ \boldsymbol{v} \in H_0^1(\Omega)^d. \tag{32}$$

Formal computations lead to:

$$\boldsymbol{a}(\boldsymbol{v},\boldsymbol{v}) = \int_\Omega \boldsymbol{v}\cdot\boldsymbol{v} + \nu\delta t \int_\Omega |\nabla\boldsymbol{v}|^2 \geq \min\{1,\nu\delta t\}\ \|\boldsymbol{v}\|_{H^1}^2,\ \ \forall\boldsymbol{v} \in H_0^1(\Omega)^d,$$

and

$$|L(\boldsymbol{v})| \leq (\|\boldsymbol{v}^n\|_{H^1} + \delta t\ \|\boldsymbol{v}^n\|_{L^\infty}\|\boldsymbol{v}^n\|_{H^1})\,\|\boldsymbol{v}\|_{H^1},\ \ \forall\ \boldsymbol{v} \in H_0^1(\Omega)^d.$$

By the Lax-Milgram theorem [17, 35], there exists a unique $\tilde{\boldsymbol{v}}^{n+1} \in H_0^1(\Omega)^d$, solution of (29) and $\boldsymbol{v}^{n+1} = \mathbb{P}^{div,0}(\tilde{\boldsymbol{v}}^{n+1})$. The spatial approximation of these solutions is detailed in next subsection.

3.2 Spatial discretization

For simplicity, this part takes place in dimension $d = 3$, but can be generalized in general dimension. At a fixed spatial resolution $j \geq j_{min}$, the numerical solutions $\tilde{\boldsymbol{v}}^n$ and $\boldsymbol{v}^n$ of (29-30) are searched as the following linear combination of wavelets:

$$\tilde{\boldsymbol{v}}_j^n = \sum_{\epsilon=1}^{3}\left(\sum_{j_{min}-1\leq|\boldsymbol{j}|<j}\sum_{\boldsymbol{k}} \tilde{d}_{\boldsymbol{j},\boldsymbol{k}}^{n,\epsilon}\,\Psi_{\boldsymbol{j},\boldsymbol{k}}^{\epsilon}\right) \text{ and } \boldsymbol{v}_j^n = \sum_{\epsilon=1}^{2}\left(\sum_{j_{min}-1\leq|\boldsymbol{j}|<j}\sum_{\boldsymbol{k}} d_{\boldsymbol{j},\boldsymbol{k}}^{div,n,\epsilon}\Psi_{\boldsymbol{j},\boldsymbol{k}}^{div,0,\epsilon}\right),$$

where for $\epsilon = 1,2,3$, $\Psi_{\boldsymbol{j},\boldsymbol{k}}^{\epsilon}$ denote the usual tensor-product wavelets of the space $\mathbf{V}_j^{dd}$ introduced in (20), whose (vector) scaling functions $\Phi_{j,\boldsymbol{k}}^{\epsilon}$ are recalled below:

$$\Phi_{j,\boldsymbol{k}}^1 = \begin{bmatrix}\varphi_{j,k_1}^d\otimes\varphi_{j,k_2}^{00}\otimes\varphi_{j,k_3}^{00}\\ 0\\ 0\end{bmatrix}, \Phi_{j,\boldsymbol{k}}^2 = \begin{bmatrix}0\\ \varphi_{j,k_1}^{00}\otimes\varphi_{j,k_2}^{d}\otimes\varphi_{j,k_3}^{00}\\ 0\end{bmatrix}, \Phi_{j,\boldsymbol{k}}^3 = \begin{bmatrix}0\\ 0\\ \varphi_{j,k_1}^{00}\otimes\varphi_{j,k_2}^{00}\otimes\varphi_{j,k_3}^{d}\end{bmatrix}.$$

For the wavelet basis $\Psi_{\boldsymbol{j},\boldsymbol{k}}^{\epsilon}$ we adopted the convention that at index $j_{min}-1$, the wavelets have to be replaced by scaling functions:

$$\Psi_{j_{min}-1,\boldsymbol{k}}^{\epsilon} = \Phi_{j_{min},\boldsymbol{k}}^{\epsilon} \qquad \text{and} \qquad \Psi_{j_{min}-1,\boldsymbol{k}}^{div,0,\epsilon} = \Phi_{j_{min},\boldsymbol{k}}^{div,0,\epsilon}.$$

We use a Galerkin method to compute the set of coefficients $(\tilde{d}_{\boldsymbol{j},\boldsymbol{k}}^{n+1,\epsilon})$ and $(d_{\boldsymbol{j},\boldsymbol{k}}^{div,n+1,\epsilon})$ on these wavelet bases. The numerical resolution of (29-30) thus yields to the

resolution of two linear systems:

$$\mathbb{M}_j(\tilde{d}^{n+1,\epsilon}_{\boldsymbol{j},\boldsymbol{k}}) = \mathbb{A}_j\left((d^{n,\epsilon}_{\boldsymbol{j},\boldsymbol{k}}) + \delta t(h^{n,\epsilon}_{\boldsymbol{j},\boldsymbol{k}})\right), \tag{33}$$

and

$$\mathbb{M}^{div}_j(d^{div,n+1,\epsilon}_{\boldsymbol{j},\boldsymbol{k}}) = \left((\langle \tilde{v}^{n+1}_j, \Psi^{div,0,\epsilon}_{\boldsymbol{j},\boldsymbol{k}}\rangle)\right), \tag{34}$$

where $d^{n,\epsilon}_{\boldsymbol{j},\boldsymbol{k}}$ and $h^{n,\epsilon}_{\boldsymbol{j},\boldsymbol{k}}$ are respectively the coefficients of the projection of $\boldsymbol{v}^n$ and $(\boldsymbol{v}^n \cdot \nabla)\boldsymbol{v}^n$ onto the basis $\{\Psi^{\epsilon}_{\boldsymbol{j},\boldsymbol{k}}\}$. The nonlinear term $(\boldsymbol{v}^n \cdot \nabla)\boldsymbol{v}^n$ is computed at grid collocation points before its projection onto the wavelet space, where the gradient operator ∇ is approximated using a finite difference method of the same order as the scaling function φ^1 polynomial approximation order [23]. Likewise, $\mathbb{A}_j$ and $\mathbb{M}_j$ correspond respectively to the matrices of the projection of the identity operator and $1 - \delta t\Delta$ onto this wavelet space, and $\mathbb{M}^{div}_j$ denotes the divergence-free wavelet basis Gramian matrix. In practice, one can take advantage of the tensor product construction of the above wavelet bases, thus to reduce the storage and the numerical complexity of vector-matrix multiplication in (33) and (34). For the numerical computation and properties of these matrices and projections, the reader is referred to [1, 21, 23].

The numerical schemes (29 – 30) and (33 – 34) are stable and consistent with the Navier-Stokes equations (27). This can be deduced from the numerical error estimations.

3.3 Numerical error estimations

Let $\boldsymbol{v}^n_j$ be the numerical solution of (33) and (34). If the initial condition $\boldsymbol{v}^0$ is regular enough, the following lemma is verified:

Lemma 1 *For $\boldsymbol{v}^n_j$ an approximated solution of* (30) *given by* (33) *and* (34)*, with an appropriated time step δt, we have:*

$$\|\boldsymbol{v}^n_j\|^2_{L^2} \leq C(\boldsymbol{v}^0, \nu) \tag{35}$$

and

$$\nu\delta t \sum_{k=1}^{n} \|\nabla \boldsymbol{v}^k_j\|^2_{L^2} \leq C(\boldsymbol{v}^0, \nu), \tag{36}$$

where $C(\boldsymbol{v}^0, \nu)$ is a positive constant depending only on the initial data.

Proof To prove the lemma, it suffices to show that:

$$\|\boldsymbol{v}_j^n\|_{L^2}^2 + \nu\delta t C \sum_{k=1}^{n} \|\nabla \boldsymbol{v}_j^k\|_{L^2}^2 \leq C(\boldsymbol{v}^0, \nu), \tag{37}$$

and this is done by induction with similar arguments as in the proof of Lemma 5.9 of [35]. Let us introduce a constant $C(\boldsymbol{v}^0, \nu)$ such that:

$$C(\boldsymbol{v}^0, \nu) = \|\boldsymbol{v}^0\|_{L^2}^2 + \delta t^2 2^{jd} \|\boldsymbol{v}^0\|_{L^2}^2 \|\nabla \boldsymbol{v}^0\|_{L^2}^2. \tag{38}$$

Now, we assume that (37) holds for some $n \geq 0$. Then, using (31) and (32), the variational formulation for the solution $\tilde{\boldsymbol{v}}_j^{n+1}$ reads:

$$a(\tilde{\boldsymbol{v}}_j^{n+1}, \boldsymbol{v}) = L(\boldsymbol{v}), \ \ \forall\ \boldsymbol{v} \in \mathbf{V}_j^d, \ \ \text{for } j > j_{min}. \tag{39}$$

Since $\nabla \cdot \boldsymbol{v}_j^{n+1} = 0$, taking $2\boldsymbol{v}_j^{n+1}$ as a test function in (39) and replacing $\tilde{\boldsymbol{v}}_j^{n+1}$ by its ex (28) leads to:

$$\|\boldsymbol{v}_j^{n+1}\|_{L^2}^2 - \|\boldsymbol{v}_j^n\|_{L^2}^2 + \|\boldsymbol{v}_j^{n+1} - \boldsymbol{v}_j^n\|_{L^2}^2 + 2\nu\delta t \|\nabla \boldsymbol{v}_j^{n+1}\|_{L^2}^2 = -2\delta t \langle (\boldsymbol{v}_j^n \cdot \nabla)\boldsymbol{v}_j^n, \boldsymbol{v}_j^{n+1} \rangle \tag{40}$$

Otherwise, we have:

$$\begin{aligned}
\delta t \langle (\boldsymbol{v}_j^n \cdot \nabla)\boldsymbol{v}_j^n, \boldsymbol{v}_j^{n+1} \rangle &= \delta t \langle (\boldsymbol{v}_j^n \cdot \nabla)\boldsymbol{v}_j^n, \boldsymbol{v}_j^{n+1} - \boldsymbol{v}_j^n \rangle \leq \delta t \|\boldsymbol{v}_j^n\|_{L^\infty} \|\nabla \boldsymbol{v}_j^n\|_{L^2} \|\boldsymbol{v}_j^{n+1} - \boldsymbol{v}_j^n\|_{L^2} \\
&\leq \frac{\delta t^2}{2} \|\boldsymbol{v}_j^n\|_{L^\infty}^2 \|\nabla \boldsymbol{v}_j^n\|_{L^2}^2 + \frac{1}{2} \|\boldsymbol{v}_j^{n+1} - \boldsymbol{v}_j^n\|_{L^2}^2
\end{aligned}$$

Thus, collecting these estimations together, we deduce that:

$$\|\boldsymbol{v}_j^{n+1}\|_{L^2}^2 - \|\boldsymbol{v}_j^n\|_{L^2}^2 + 2\nu\delta t \|\nabla \boldsymbol{v}_j^{n+1}\|_{L^2}^2 \leq \delta t^2 \|\boldsymbol{v}_j^n\|_{L^\infty}^2 \|\nabla \boldsymbol{v}_j^n\|_{L^2}^2. \tag{41}$$

We recall that $\boldsymbol{v}_j^n \in \mathbf{V}_j^d$ for $j > j_{min}$. As we are in finite space dimension, we have:

$$\|\boldsymbol{v}_j^n\|_{L^\infty}^2 \leq 2^{jd} \|\boldsymbol{v}_j^n\|_{L^2}^2, \tag{42}$$

and Equation (41) becomes:

$$\|\boldsymbol{v}_j^{n+1}\|_{L^2}^2 - \|\boldsymbol{v}_j^n\|_{L^2}^2 + 2\nu\delta t \|\nabla \boldsymbol{v}_j^{n+1}\|_{L^2}^2 \leq \delta t^2 2^{jd} \|\boldsymbol{v}_j^n\|_{L^2}^2 \|\nabla \boldsymbol{v}_j^n\|_{L^2}^2. \tag{43}$$

For $n = 1$, (41) reads:

$$\|\boldsymbol{v}_j^1\|_{L^2}^2 + 2\nu\delta t \|\nabla \boldsymbol{v}_j^1\|_{L^2}^2 \leq \|\boldsymbol{v}_j^0\|_{L^2}^2 + \delta t^2 2^{jd} \|\boldsymbol{v}_j^0\|_{L^2}^2 \|\nabla \boldsymbol{v}_j^0\|_{L^2}^2. \tag{44}$$

This is the statement of the lemma with:

$$C(\boldsymbol{v}^0, \nu) \geq \|\boldsymbol{v}_j^0\|_{L^2}^2 + \delta t^2 2^{jd} \|\boldsymbol{v}_j^0\|_{L^2}^2 \|\nabla \boldsymbol{v}_j^0\|_{L^2}^2. \tag{45}$$

Summation over n in (41) leads to:

$$\|\boldsymbol{v}_j^{n+1}\|_{L^2}^2 - \|\boldsymbol{v}_j^0\|_{L^2}^2 + 2\nu\delta t \sum_{k=0}^{n} \|\nabla \boldsymbol{v}_j^{k+1}\|_{L^2}^2 \leq \delta t^2 2^{jd} \sum_{k=0}^{n} \|\boldsymbol{v}_j^k\|_{L^2}^2 \|\nabla \boldsymbol{v}_j^k\|_{L^2}^2, \quad (46)$$

and rewritten this, we get:

$$\|\boldsymbol{v}_j^{n+1}\|_{L^2}^2 + 2\nu\delta t \|\nabla \boldsymbol{v}_j^{n+1}\|_{L^2}^2 + 2\nu\delta t \sum_{k=1}^{n} \|\nabla \boldsymbol{v}_j^k\|_{L^2}^2 \leq C(\boldsymbol{v}^0, \nu) + \delta t^2 2^{jd} C(\boldsymbol{v}^0, \nu) \sum_{k=1}^{n} \|\nabla \boldsymbol{v}_j^k\|_{L^2}^2,$$

which implies

$$\|\boldsymbol{v}_j^{n+1}\|_{L^2}^2 + 2\nu\delta t \|\nabla \boldsymbol{v}_j^{n+1}\|_{L^2}^2 + \delta t[2\nu - \delta t 2^{jd} C(\boldsymbol{v}^0, \nu)] \sum_{k=1}^{n} \|\nabla \boldsymbol{v}_j^k\|_{L^2}^2 \leq C(\boldsymbol{v}^0, \nu) \quad (47)$$

From (47), to end the proof of the lemma, we take δt small enough such that:

$$\delta t 2^{jd} C(\boldsymbol{v}^0, \nu) < 2\nu. \quad (48)$$

□

Now we will analyze the behavior of the local error $\boldsymbol{e}^n = \boldsymbol{v}(t_n) - \boldsymbol{v}^n$, where $\boldsymbol{v}$ is a smooth solution of the exact Navier-Stokes equations (27) and $\boldsymbol{v}^n$ the numerical solution of (29) and (30). With the help of the Lemma 1, we get:

Proposition 2 *Let $\boldsymbol{v} \in H^2(0,T; L^2(\Omega)^d) \cap C^0(0,T; W^{1,+\infty}(\Omega)^d \cap H_0^1(\Omega)^d)$ be a solution of* (27) *and $\boldsymbol{v}^n$ a solution of* (29 − 30)*. Denoting by $\boldsymbol{e}^n = \boldsymbol{v}(t_n) - \boldsymbol{v}^n$ the local error, we have:*

$$\max_n \|\boldsymbol{e}^n\|_{L^2(\Omega)^d}^2 \xrightarrow[\delta t \to 0]{} 0. \quad (49)$$

Proof According to (29) and (30), we see that:

$$\boldsymbol{v}(t_{n+1}) - \boldsymbol{v}(t_n) - \delta t \nu \Delta \boldsymbol{v}(t_{n+1}) + \delta t (\boldsymbol{v}(t_n) \cdot \nabla)\boldsymbol{v}(t_n) = \delta t \boldsymbol{\epsilon}^{n+1} - \delta t \nabla p(t_n), \quad (50)$$

where $\boldsymbol{\epsilon}^n$ denotes the consistency error. Since $\nabla \cdot \boldsymbol{e}^{n+1} = 0$, taking $2\boldsymbol{e}^{n+1}$ as test function in the variational formulations and using similar arguments as in the proof of Lemma 1 allow to get:

$$\begin{aligned} \|\boldsymbol{e}^{n+1}\|_{L^2}^2 &- \|\boldsymbol{e}^n\|_{L^2}^2 + \|\boldsymbol{e}^{n+1} - \boldsymbol{e}^n\|_{L^2}^2 + 2\delta t \nu \|\nabla \boldsymbol{e}^{n+1}\|_{L^2}^2 \\ &\leq 2\delta t \|\boldsymbol{v}^n\|_{L^\infty} \|\nabla \boldsymbol{e}^n\|_{L^2} \|\boldsymbol{e}^{n+1} - \boldsymbol{e}^n\|_{L^2} + 2\delta t \|\boldsymbol{e}^n\|_{L^2} \|\nabla \boldsymbol{v}(t_n)\|_{L^\infty} \|\boldsymbol{e}^{n+1}\|_{L^2} \\ &+ 2\delta t \langle \boldsymbol{\epsilon}^{n+1}, \boldsymbol{e}^{n+1} \rangle \end{aligned} \quad (51)$$

Poincaré and Young's inequalities lead to:

$$\begin{aligned} \|\boldsymbol{e}^{n+1}\|_{L^2}^2 - \|\boldsymbol{e}^n\|_{L^2}^2 + \delta t \nu \|\nabla \boldsymbol{e}^{n+1}\|_{L^2}^2 &\leq \delta t^2 \|\boldsymbol{v}^n\|_{L^\infty}^2 \|\nabla \boldsymbol{e}^n\|_{L^2}^2 \\ &+ \frac{C(\Omega)^2 \delta t}{\nu} \|\boldsymbol{e}^n\|_{L^2}^2 \|\nabla \boldsymbol{v}(t_n)\|_{L^\infty}^2 + 2\delta t \langle \boldsymbol{\epsilon}^{n+1}, \boldsymbol{e}^{n+1} \rangle \end{aligned} \quad (52)$$

Since $\nabla \cdot \boldsymbol{e}^n = 0$, using (50) we have:

$$\delta t \langle \boldsymbol{\epsilon}^{n+1}, \boldsymbol{e}^{n+1} \rangle = \langle \boldsymbol{v}(t_{n+1}) - \boldsymbol{v}(t_n) - \delta t \nu \Delta \boldsymbol{v}(t_{n+1}) + \delta t (\boldsymbol{v}(t_n) \cdot \nabla)\boldsymbol{v}(t_n), \boldsymbol{e}^{n+1} \rangle, \quad (53)$$

and replacing $-\Delta \boldsymbol{v}(t_{n+1})$ by

$$-\nu\Delta \boldsymbol{v}(t_{n+1}) = -\partial_t \boldsymbol{v}(t_{n+1}) - (\boldsymbol{v}(t_{n+1})\cdot\nabla)\boldsymbol{v}(t_{n+1}) - \nabla p(t_{n+1}), \tag{54}$$

we obtain:

$$\begin{aligned}
&\delta t\langle \boldsymbol{\epsilon}^{n+1}, \boldsymbol{e}^{n+1}\rangle \\
&= \langle \boldsymbol{v}(t_{n+1}) - \boldsymbol{v}(t_n) - \delta t\partial_t \boldsymbol{v}(t_{n+1}) + \delta t[(\boldsymbol{v}(t_n)\cdot\nabla)\boldsymbol{v}(t_n) - (\boldsymbol{v}(t_{n+1})\cdot\nabla)\boldsymbol{v}(t_{n+1})], \boldsymbol{e}^{n+1}\rangle \\
&= \delta t\langle \frac{1}{\delta t}\int_{t_n}^{t_{n+1}} (t_n - t)\partial_{tt}\boldsymbol{v}(t)dt - \int_{t_n}^{t_{n+1}} \partial_t[(\boldsymbol{v}(t)\cdot\nabla)\boldsymbol{v}(t)]dt, \boldsymbol{e}^{n+1}\rangle \\
&\leq \left(\frac{\delta t^{3/2}}{\sqrt{3}}\|\partial_{tt}\boldsymbol{v}\|_{L^2(t_n,t_{n+1};L^2)} + \delta t^{3/2}\|\partial_t[(\boldsymbol{v}\cdot\nabla)\boldsymbol{v}]\|_{L^2(t_n,t_{n+1};L^2)}\right)\|\boldsymbol{e}^{n+1}\|_{L^2}
\end{aligned} \tag{55}$$

Again, using Young's inequality we have:

$$\begin{aligned}
2\delta t\langle \boldsymbol{\epsilon}^{n+1}, \boldsymbol{e}^{n+1}\rangle \leq\ & \frac{4C(\Omega)^2\delta t^2}{3\nu}\|\partial_{tt}\boldsymbol{v}\|^2_{L^2(t_n,t_{n+1};L^2)} + \frac{4C(\Omega)^2\delta t^2}{\nu}\|\partial_t[(\boldsymbol{v}\cdot\nabla)\boldsymbol{v}]\|^2_{L^2(t_n,t_{n+1};L^2)} \\
&+\frac{\nu\delta t}{2}\|\nabla\boldsymbol{e}^{n+1}\|^2_{L^2},
\end{aligned}$$

and from the maximum principle and regularity of the solution of elliptic problem, we infer that:

$$\|\boldsymbol{v}^n\|_{L^\infty} \lesssim \|\boldsymbol{v}_j^n\|_{L^\infty}.$$

Thus, (52) becomes:

$$\begin{aligned}
\|\boldsymbol{e}^{n+1}\|^2_{L^2} - \|\boldsymbol{e}^n\|^2_{L^2} + \frac{\delta t\nu}{2}\|\nabla\boldsymbol{e}^{n+1}\|^2_{L^2} \leq\ & \delta t^2 2^{jd}\|\boldsymbol{v}_j^n\|^2_{L^2}\|\nabla\boldsymbol{e}^n\|^2_{L^2} + \frac{C(\Omega)^2\delta t}{\nu}\|\boldsymbol{e}^n\|^2_{L^2}\|\nabla\boldsymbol{v}(t_n)\|^2_{L^\infty} \\
&+ \frac{4C(\Omega)^2\delta t^2}{3\nu}\|\partial_{tt}\boldsymbol{v}\|^2_{L^2(t_n,t_{n+1};L^2)} \\
&+ \frac{4C(\Omega)^2\delta t^2}{\nu}\|\partial_t[(\boldsymbol{v}\cdot\nabla)\boldsymbol{v}]\|^2_{L^2(t_n,t_{n+1};L^2)}
\end{aligned}$$

Summation over n in (52) shows that:

$$\begin{aligned}
\|\boldsymbol{e}^{n+1}\|^2_{L^2} - \|\boldsymbol{e}^0\|^2_{L^2} + \frac{\delta t\nu}{2}\sum_{k=1}^{n+1}\|\nabla\boldsymbol{e}^k\|^2_{L^2} \leq\ & \delta t^2 2^{jd}\sum_{k=0}^{n}\|\boldsymbol{v}_j^k\|^2_{L^2}\|\nabla\boldsymbol{e}^k\|^2_{L^2} \\
&+C_1\delta t\sum_{k=0}^{n}\|\boldsymbol{e}^k\|^2_{L^2} + C_2\delta t^2,
\end{aligned}$$

with

$$C_1 = \frac{C(\Omega)^2}{\nu}\|\nabla\boldsymbol{v}\|^2_{L^\infty(0,T,L^\infty)}, C_2 = \frac{4C(\Omega)^2}{3\nu}\|\partial_{tt}\boldsymbol{v}\|^2_{L^2(0,T;L^2)} + \frac{4C(\Omega)^2}{\nu}\|\partial_t[(\boldsymbol{v}\cdot\nabla)\boldsymbol{v}]\|^2_{L^2(0,T;L^2)}$$

Since $\|\boldsymbol{v}_j^k\|^2_{L^2} \leq C(\boldsymbol{v}^0,\nu)$ according to Lemma 1, we have:

$$\|\boldsymbol{e}^{n+1}\|_{L^2}^2 + \frac{\delta t\nu}{2}\|\nabla \boldsymbol{e}^{n+1}\|_{L^2}^2 + (\frac{\delta t\nu}{2} - \delta t^2 2^{jd} C(\boldsymbol{v}^0, \nu)) \sum_{k=1}^{n} \|\nabla \boldsymbol{e}^k\|_{L^2}^2 \leq \lambda_0 + C_1 \delta t \sum_{k=0}^{n} \|\boldsymbol{e}^k\|_{L^2}^2 + C_2 \delta t^2,$$

where:

$$\lambda_0 = \|\boldsymbol{e}^0\|_{L^2}^2 + \delta t^2 2^{jd} C(\boldsymbol{v}^0, \nu)\|\nabla \boldsymbol{e}^0\|_{L^2}^2.$$

Then, choosing δt small enough such that:

$$\frac{\nu}{2} - \delta t 2^{jd} C(\boldsymbol{v}^0, \nu) > 0, \tag{56}$$

by the discrete Gronwall lemma, see [35, 38], we deduce that:

$$\|\boldsymbol{e}^n\|_{L^2}^2 \leq \left(\lambda_0 + C_2 \delta t^2\right) \exp(C_1 T) \tag{57}$$

□

For the numerical error $\boldsymbol{e}_j^n = \boldsymbol{v}(t_n) - \boldsymbol{v}_j^n$, we can write:

$$\|\boldsymbol{e}_j^n\|_{L^2}^2 \leq 2\left(\|\boldsymbol{v}(t_n) - \boldsymbol{v}^n\|_{L^2}^2 + \|\boldsymbol{v}^n - \boldsymbol{v}_j^n\|_{L^2}^2\right),$$

and

$$\|\boldsymbol{v}^n - \boldsymbol{v}_j^n\|_{L^2}^2 \leq C\|\boldsymbol{v}^n - \mathbb{P}_j^{div,0}(\boldsymbol{v}^n)\|_{L^2}^2.$$

Thus, due to the Jackson estimation (24) and Proposition 2, we obtain the following convergence result:

$$\|\boldsymbol{e}_j^n\|_{L^2(\Omega)^d}^2 \xrightarrow[\delta t \to 0, \delta x \to 0]{} 0. \tag{58}$$

4 Numerical results

We present in this section numerical results on the simulation of the Navier-Stokes equations, obtained using the time and spatial discretization (29 – 30) and (33 – 34). These results will be compared to those of the literature for method validation.

4.1 Divergence free wavelet illustration

We start by presenting the wavelet bases generators introduced in Section 2.1, used in all the numerical experiments that follow. We chose as scaling function generators $(\varphi^1, \tilde{\varphi}^1)$, the biorthogonal splines of order four: $r = \tilde{r} = 4$. This corresponds to four vanishing moments for each wavelet generator ψ^1 and $\tilde{\psi}^1$. We plot in Figure 1 the

graph of φ^1 and its derivative that satisfies $(\varphi^1(x))' = \varphi^0(x) - \varphi^0(x-1)$. Thus, the scaling function φ^0 can reproduce polynomials up to order 3 (or equivalently of degree up to 2). Figure 2 shows the graph of the wavelet generators ψ^1 and $(\psi^1)' = 4\psi^0$. The biorthogonal functions $(\tilde{\varphi}^1, \tilde{\psi}^1)$ are plotted in Figure 3.

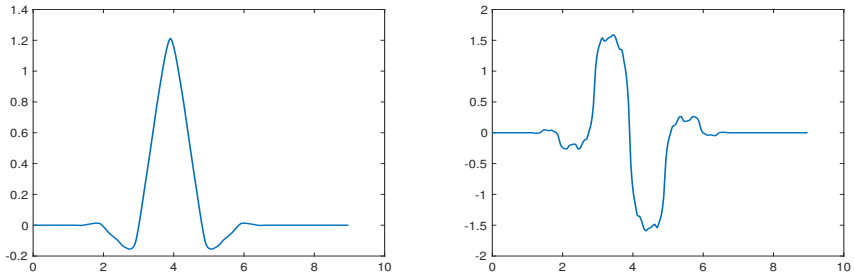

(a) φ^1 (b) $(\varphi^1)'$

Fig. 1 Primal biorthogonal spline scaling function generator φ^1 (left) and its derivative $(\varphi^1(x))' = \varphi^0(x) - \varphi^0(x-1)$ (right) with order parameters $r = \tilde{r} = 4$.

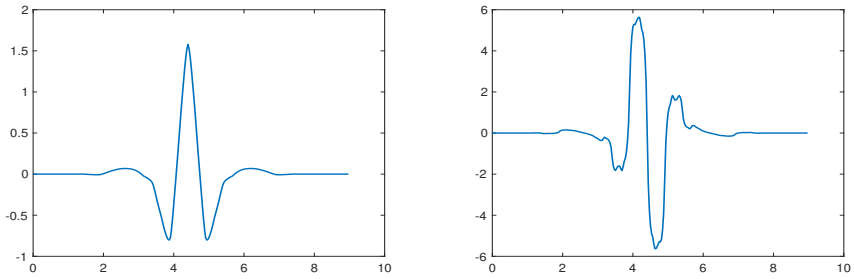

(a) ψ^1 (b) $4\psi^0$

Fig. 2 Primal biorthogonal spline wavelet generator ψ^1 (left) and its derivative $(\psi^1(x))' = 4\psi^0(x)$ (right) with order parameters $r = \tilde{r} = 4$.

As mentioned in Section 2.2, the above scaling functions allow to construct, in dimension 3, three divergence-free scaling function generators, defined by (10 – 12). We plot in Figure 4 the isosurface of the magnitude of some internal scaling functions $\Phi^{div,1}_{j,\boldsymbol{k}}$, $\Phi^{div,2}_{j,\boldsymbol{k}}$ and $\Phi^{div,3}_{j,\boldsymbol{k}}$, where for a vector function $\boldsymbol{v} = (v_1, v_2, v_3)$, the magnitude

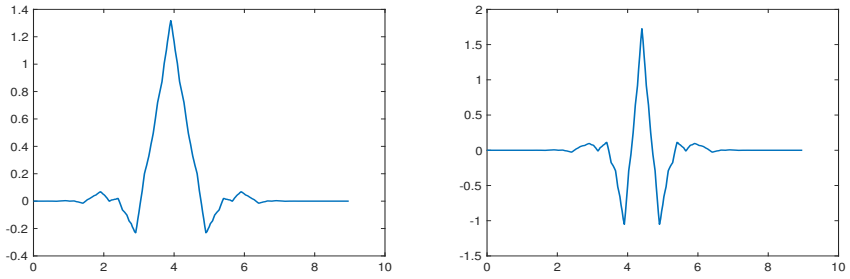

(a) $\tilde{\varphi}^1$ (b) $\tilde{\psi}^1$

Fig. 3 Dual biorthogonal spline scaling function generator $\tilde{\varphi}^1$ (left) and the dual wavelet generator $\tilde{\psi}^1$ (right) with order parameters $r = \tilde{r} = 4$.

is defined as: $|\boldsymbol{v}| = \sqrt{v_1^2 + v_2^2 + v_3^2}$. Likewise, the corresponding divergence-free wavelet generators magnitude isosurfaces are shown in Figure 4.

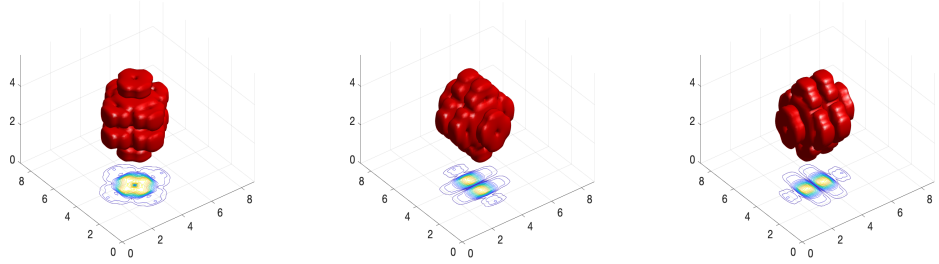

(a) $|\Phi^{div,1}_{j,\boldsymbol{k}}| = 0.2$ (b) $|\Phi^{div,2}_{j,\boldsymbol{k}}| = 0.2$ (c) $|\Phi^{div,3}_{j,\boldsymbol{k}}| = 0.2$

Fig. 4 Divergence-free scaling functions magnitude isosurface for biorthogonal spline generators $(\varphi^1, \tilde{\varphi}^1)$ of order 4

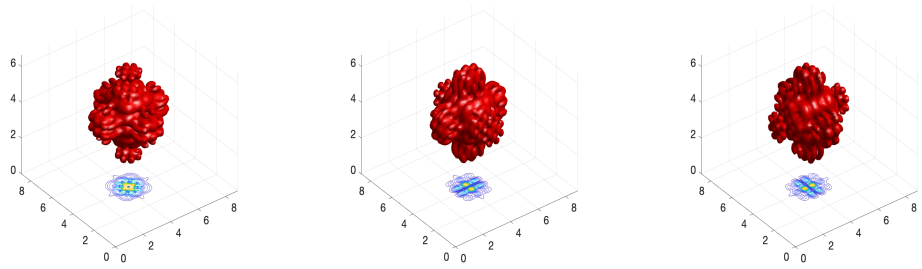

(a) $|\Psi^{div,1}_{\boldsymbol{j},\boldsymbol{k}}| = 0.4$ (b) $|\Psi^{div,2}_{\boldsymbol{j},\boldsymbol{k}}| = 0.4$ (c) $|\Psi^{div,3}_{\boldsymbol{j},\boldsymbol{k}}| = 0.4$

Fig. 5 Divergence-free wavelets magnitude isosurfacef or biorthogonal spline generators $(\varphi^1, \tilde{\varphi}^1)$ of order 4.

4.2 Analyses of time and space convergence rates

In this part we study the time and space convergence rates provided by the divergence-free wavelet based projection method (29 – 30)-(33 – 34) introduced in Section 3. We present below two experiments on analytical solutions.

The spatial discretization of the divergence-free wavelet based projection method uses the scaling function and wavelet generators of Section 4.1. In practice, one time iteration step (33 – 34) split into the following steps:

Step 0: Start with an initial velocity $\boldsymbol{v}^0(x) = \boldsymbol{v}(x,0)$ defined on dyadic grid points at space resolution $j > j_{jmin}$.
- Compute its wavelet coefficients $[d^{0,\epsilon}_{\boldsymbol{j},\boldsymbol{k}}]$.
- Compute the nonlinear term $(\boldsymbol{v}^0 \cdot \nabla)\boldsymbol{v}^0$ using a fourth order finite difference scheme, and its wavelet coefficients $[h^{0,\epsilon}_{\boldsymbol{j},\boldsymbol{k}}]$ in $\mathbf{V}^d_j$.

For $1 \leq n \leq N$, repeat:

Step 1: Find $[\tilde{d}^{n+1,\epsilon}_{\boldsymbol{j},\boldsymbol{k}}]$ solution of (33).

Step 2: Find $[d^{div,n+1,\epsilon}_{\boldsymbol{j},\boldsymbol{k}}]$ solution of (34).

Step 3: Compute $[d^{n+1,\epsilon}_{\boldsymbol{j},\boldsymbol{k}}]$ from $[\boldsymbol{d}^{div,n+1,\epsilon}_{\boldsymbol{j},\boldsymbol{k}}]$ using a change of basis [22] and extrapolate $\boldsymbol{v}^{n+1}_j$ at grid points to compute the nonlinear term, and update.

Remark 1 An explicite optimal preconditioner is known for the matrices $\mathbb{M}_j$ and $\mathbb{M}^{div}_j$, see [6, 22] and references therein. Therefore we use a preconditioned conjugate gradient method to solve systems (33) and (34). Moreover, due to the tensor product

construction of wavelet bases, the matrix-vector product in (33) and (34) only requires the use of one-dimensional basis stiffness matrices [21, 23]. Therefore, the numerical complexity to solve (33) and (34) is about $O(N_j^4)$, with N_j the dimension of the one-dimensional space V_j^1.

The time discretization convergence rate of the proposed divergence-free wavelet based projection method is studied on a designed solution $(\boldsymbol{v}, p)$ defined by:

$$\begin{cases} v_1(x,y,z,t) = 2e^{-t}(x^4 + x^2 - 2x^3)(2y + 4y^3 - 6y^2)(2z + 4z^3 - 6z^2), \\ v_2(x,y,z,t) = -e^{-t}(2x + 4x^3 - 6x^2)(y^4 + y^2 - 2y^3)(2z + 4z^3 - 6z^2), \\ v_3(x,y,z,t) = -e^{-t}(2x + 4x^3 - 6x^2)(2y + 4y^3 - 6y^2)(z^4 + z^2 - 2z^3), \\ p(x,y,t) = \cos(t)[(x^2 - x)(y^2 - y)(z^2 - z)]^2. \end{cases} \tag{59}$$

This solution satisfies Dirichlet homogeneous boundary conditions $\boldsymbol{v}_{|\partial\Omega} = 0$, where $\Omega = [0,1]^3$ and appropriate forcing terms $\boldsymbol{f}$ are added to ensure that (59) is an exact solution of (27). Since the quadrature formula for the projection onto $\mathbf{V}_j^d$ is exact up to order 3, which is the polynomial reproduction order of the scaling function φ^0, the spatial discretization error for the solution (59) is negligible compared to the time discretization error for $\delta t < 0.1$. Tab. 1 shows different errors between the exact solution projected onto $\mathbf{V}_j^d$ (with a space resolution fixed at $j = 7$ and viscosity $\nu = 2^{-j}$), and the numerical solution of (29 – 30)-(33 – 34), in terms of the discretization time step δt. For each norm considered, the expected first order convergence rate is obtained.

Going further, we also analyzed the convergence rate of a second order numerical scheme: Crank-Nicholson for the diffusion part and Adams-Bashforth for the non-linear term [23]. The results of this experiment are given in Tab. 2, where again the expected order is achieved.

Backward-Euler				
δt	0.05	0.025	0.0166	Order
L_∞-error	7.2549E^{-5}	3.6427E^{-5}	2.4318E^{-5}	0.99159
L_2-error	2.9129E^{-5}	1.4626E^{-5}	9.7643E^{-6}	0.99157
H^1-error	2.9031E^{-4}	1.4576E^{-4}	9.7312E^{-5}	0.99159

Table 1 Time discretization relative errors according to the time step δt, for the solution (59) at final time $T = 1$, $j = 7$ and $\nu = 2^{-j}$.

Similarly, we investigate the spatial projection error convergence rate of the proposed divergence-free wavelet based projection, using the following exact solution:

$$\begin{cases} v_1(x,y,z,t) = 2e^{-t}\sin^2(2\pi x)\sin(4\pi y)\sin(4\pi z), \\ v_2(x,y,z,t) = -e^{-t}\sin(4\pi x)\sin^2(2\pi y)\sin(4\pi z), \\ v_3(x,y,z,t) = -e^{-t}\sin(4\pi x)\sin(4\pi y)\sin^2(2\pi z), \\ p(x,y,t) = \cos(t)[(x^2 - x)(y^2 - y)(z^2 - z)]^2. \end{cases} \tag{60}$$

Crank-Nicholson				
δt	0.05	0.025	0.0166	Order
L_∞-error	6.1014E^{-7}	1.5292E^{-7}	6.8247E^{-8}	1.98770
L_2-error	2.4478E^{-7}	6.1226E^{-7}	2.7271E^{-8}	1.99124
H^1-error	2.4476E^{-6}	6.3177E^{-6}	3.1354E^{-7}	1.87311

Table 2 Time discretization relative errors according to the time step δt, for the solution (59) at final time $T = 1$, $j = 7$ and $\nu = 2^{-j}$.

The simulation time step is $\delta t = 0.0001$, which is very small compared to the maximal spatial resolution $j = 7$ ($\delta x = 2^{-7} = 0.0078125$) and the used kinematic viscosity $\nu = 2^{-3j}$. Tab. 3 shows the spatial error for the final time $T = 1$, using the first-order-accurate Backward-Euler time-scheme: as the solution is C^∞, the

Backward-Euler				
j	5	6	7	Order
L_2-error	1.40145E^{-3}	6.2469E^{-5}	3.2643E^{-6}	4.3729
L_∞-error	5.4952E^{-3}	2.7106E^{-4}	1.42890E^{-5}	4.2935
H^1-error	9.2027E^{-2}	7.7476E^{-3}	6.5306E^{-4}	3.5693

Table 3 Spatial discretization errors according to the resolution j, for final time $T = 1$.

convergence rate given by Tab. 3 saturates due to the number of vanishing moments of our wavelet family (equal to 3 in our spline approximation), and we lose one order for the H^1-error. Remark that the use of divergence-free wavelet basis induces no divergence error on the solution $\boldsymbol{v}_j^n$ in $\mathbf{V}_j^d$.

4.3 Simulation of 3D lid-driven flows

In addition to these preliminary studies, the present method was tested on the numerical simulation of 3D lid-driven flows in a cubic cavity $\Omega = [0,1]^3$, with Reynolds numbers $Re = 100$ and $Re = 1000$. These flows have been extensively studied in the literature and there are a lot of reference results and solutions, mainly for the two dimensional flows, see [11]. The simulations used a Matlab code and the discretization parameters are $\delta t = 0.005$ and $\delta x = 2^{-j}$, where $j = 6$ or $j = 7$ is the considered spatial resolution.

The validation is done by analyzing the flow's steady state. Specifically, we compare our simulation horizontal velocity v_x and vertical velocity v_z profiles in the middle of the cavity to the results of [11]. For $j = 6$, Figure 6 and Figure 7 show the plot of these profiles, respectively for the Reynolds numbers $Re = 100$ and $Re = 1000$. As observed, despite of some small discrepancies for $z \in [0, 0.2]$ in the

velocity component v_z, our results are in agreement with those of [11]. Moreover, as illustration we plot in Figure 8 the velocity magnitude for the simulations performed at resolution $j = 7$. As expected, this highlights the presence of a cavity central vortex.

We also analyze the divergence-free wavelet representation of the solution. For a 3D array $A = [A_{ijk}]$ of scalars, we define its magnitude as $|A| = [|A_{ijk}|]$, the array of coefficients modulus $|A_{ijk}|$. Figure 9 and Figure 10 show the map of divergence-free wavelet coefficient magnitude of the solutions, respectively for the Reynolds number $Re = 100$ and $Re = 1000$. Clearly, these figures emphasize the quality and the sparsity of such a solution approximation. This suggests the development of adaptive methods with these wavelet bases to improve the numerical complexity. As mentioned before, the actual theoretical complexity of one iteration in the method is about $O(N_j^4)$.

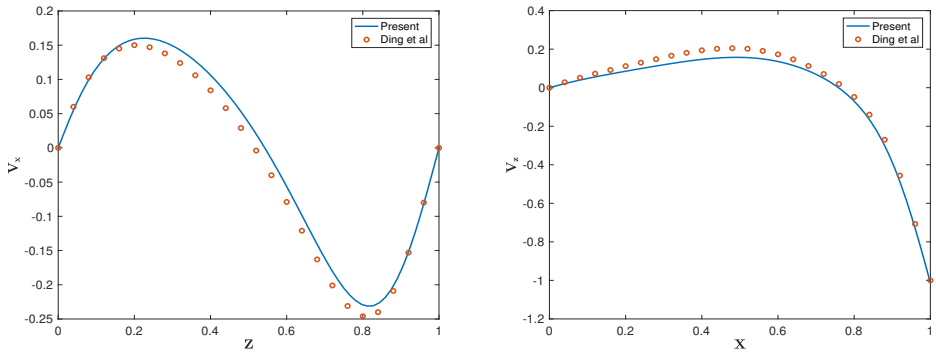

Fig. 6 Steady state velocity profile in the middle of the cavity: $v_x(0.5, 0.5, z)$ (left) and $v_z(x, 0.5, 0.5)$ (right). Solid line (present work) and circle (reference [11]) for the Reynolds number $Re = 100$ and the spatial resolution $j = 6$.

Conclusion

We presented a construction of wavelets linked by differentiation and integration that allows to construct free-slip and no-slip divergence-free wavelets on the hypercube. These divergence-free wavelets are used to provide an Helmholtz-Hodge decomposition and a change of variables in a first-order-accurate time integration for the resolution of Navier-Stokes, similar to the Gauge method. This scheme avoids the use of the projection method Poisson solver that imposes non physical boundary conditions on the pressure. Our method was tested and validated on the simulation

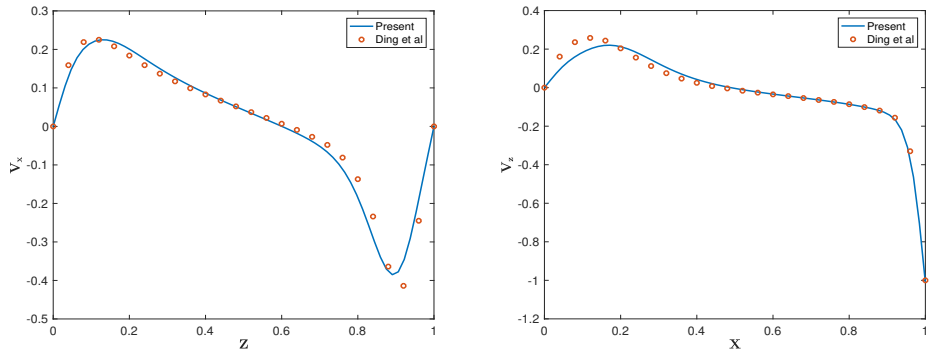

Fig. 7 Steady state velocity profile in the middle of the cavity: $v_x(0.5, 0.5, z)$ (left) and $v_z(x, 0.5, 0.5)$ (right). Solid line (present work) and circle (reference [11]) for the Reynolds number $Re = 1000$ and the spatial resolution $j = 6$.

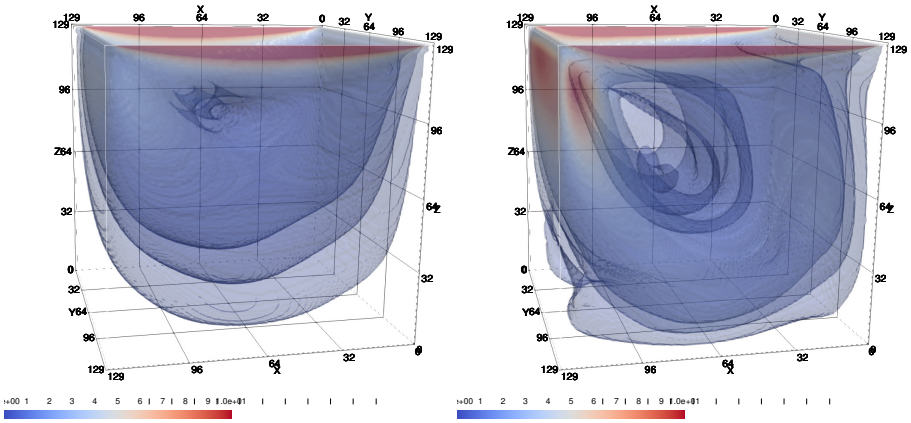

Fig. 8 Isosurface of the steady state velocity magnitude $|\boldsymbol{v}|$ for the Reynolds number $Re = 100$ (left) and $Re = 1000$ (right), at the spatial resolution $j = 7$.

of the well known 3D lid-driven cavity flow for the moderate Reynolds numbers $Re = 100$ and $Re = 1000$. From the simplicity and precision of this method, we claim that adaptive algorithms can be developed within this approach: mainly for the simulation of turbulent flows at high Reynolds number, including sub-grid models near walls.

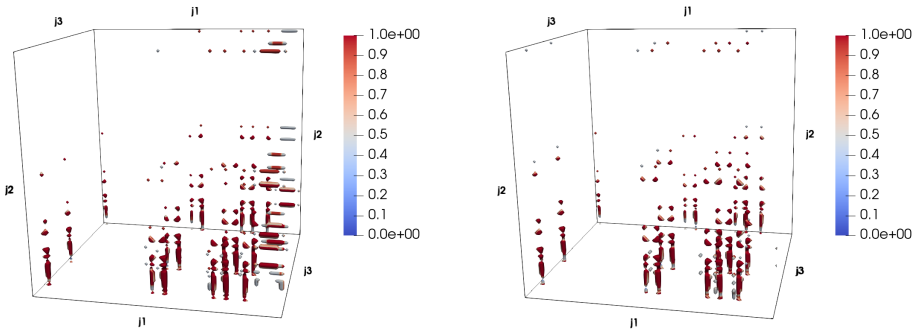

Fig. 9 Isosurface of the steady state velocity divergence-free wavelets coefficients magnitude $|d^{div,1}_{\boldsymbol{j},\boldsymbol{k}}|$ (left) and $|d^{div,2}_{\boldsymbol{j},\boldsymbol{k}}|$ (right), for the Reynolds number $Re = 100$ and $4 = j_{min} \leq j_1, j_2, j_3 \leq j = 7$.

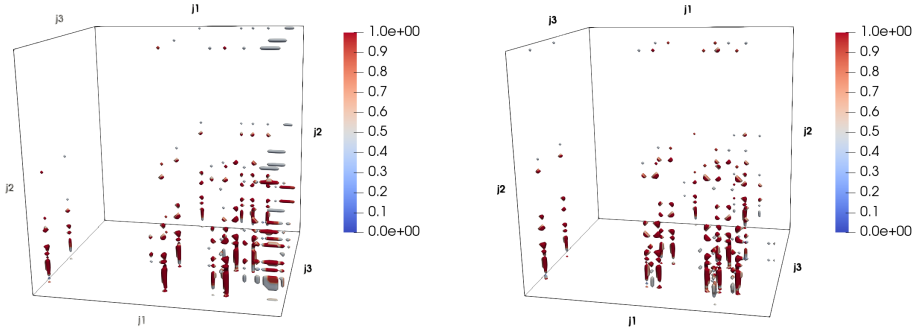

Fig. 10 Isosurface of the steady state velocity divergence-free wavelets coefficients magnitude $|d^{div,1}_{\boldsymbol{j},\boldsymbol{k}}|$ (left) and $|d^{div,2}_{\boldsymbol{j},\boldsymbol{k}}|$ (right), for the Reynolds number $Re = 1000$ and $4 = j_{min} \leq j_1, j_2, j_3 \leq j = 7$.

Appendix

Lemma 2 *[20, 26] Let $\theta \in L^2(\mathbb{R})$ be a compactly supported function, C^α-differentiable, $\alpha > 0$, and with at least one vanishing moment $\int_{\mathbb{R}} \theta = 0$. Then, there is a positive constant $C(\theta)$ such that:*

$$\forall\,(\lambda_{j,k})\in\ell^2(\mathbb{Z}^2),\ \ \|\sum_{j,k\in\mathbb{Z}}\lambda_{j,k}\theta_{j,k}\|_{L^2(\mathbb{R})}\leq C(\theta)\left(\sum_{j,k\in\mathbb{Z}}|\lambda_{j,k}|^2\right)^{1/2},\qquad(61)$$

with $\theta_{j,k}=2^{j/2}\theta(2^j.-k)$.

Proof The C^α assumption on θ leads to $|\langle\theta_{j,k},\theta_{j',k'}\rangle|\leq C2^{-|j-j'|(1/2+\alpha)}$. As θ is compactly supported, for fixed index j, k and j', we have $\langle\theta_{j,k},\theta_{j',k'}\rangle=0$ except for some k': $k'\leq M$ if $j'\leq j$ and $k'\leq M2^{(j'-j)}$ if $j'\geq j$, where M is a positive constant independent of j, j' and k. Then

$$\sup_{j,k}\sum_{j',k'}|\langle\theta_{j,k},\theta_{j',k'}\rangle|2^{(j-j')/2}<+\infty$$

and since

$$\|\sum_{j,k\in\mathbb{Z}}\lambda_{j,k}\theta_{j,k}\|^2_{L^2(\mathbb{R})}\leq\left(\sum_{j',k'}\sum_{j,k\in\mathbb{Z}}|\lambda_{j,k}|^2|\langle\theta_{j,k},\theta_{j',k'}\rangle|2^{(j-j')/2}\right)^{1/2}$$
$$\cdot\left(\sum_{j',k'}\sum_{j,k\in\mathbb{Z}}|\lambda_{j,'k'}|^2|\langle\theta_{j,k},\theta_{j',k'}\rangle|2^{(j'-j)/2}\right)^{1/2},\qquad\square$$

the lemma is proved.

References

1. G. Beylkin, *On the representation of operator in bases of compactly supported wavelets*, SIAM J. Numer. Anal., 6 (1992), pp. 1716–1740.
2. C. Canuto, R. Masson, *Stabilized wavelet approximations of the Stokes problem*, Math. of Comp., 70 (2001), pp. 1397–1416.
3. P. Charton, V. Perrier, *A Pseudo-Wavelet Scheme for the Two-Dimensional Navier-Stokes Equations*, Comp. Appl. Math., 15 (1996), pp. 137–157.
4. A.J. Chorin, *Numerical simulation of the Navier-Stokes equation*, Math. Comp., 22 (1968), pp. 745–762.
5. A. Cohen, I. Daubechies, P. Vial, *Wavelets on the Interval and Fast Wavelet Transforms*, Appl. Comput. Harmon. Anal., 1 (1993), pp. 54–81.
6. A. Cohen, R. Masson, *Wavelet methods for second order elliptic problems - preconditioning and adaptivity*, SIAM J. Sci. Comp., 21(1999), pp. 1006–1026.
7. W. Dahmen, K. Urban, J. Vorloeper, *Adaptive Wavelet Methods-Basic Concepts and Applications to the Stokes Problem*, Wavelet Analysis–Twenty Years Developments, Ding-Xuan Zhou ed., World Scientific, New Jersey, (2002), pp. 39–80.
8. E. Deriaz, V. Perrier, *Orthogonal Helmholtz decomposition in arbitrary dimension using divergence-free and curl-free wavelets*, Appl. Comput. Harmon. Anal., 26 (2009), pp. 249–269.
9. E. Deriaz, V. Perrier, *Direct Numerical Simulation of Turbulence using divergence-free wavelets*, SIAM Multis. Model. and Simul., 7 (2008), pp. 1101–1129.

10. E. Deriaz, V. Perrier, *Divergence-free and curl-free wavelets in 2D and 3D, application to turbulent flows*, J. of Turbulence, 7 (2006), pp. 1–37.
11. H.Ding, C.Shu, K.S.Yeo, D.Xub, *Numerical computation of three-dimensional incompressible viscous flows in the primitive variable form by local multiquadric differential quadrature method*, Comput. Meth. in App. Mech. and Eng., 195 (2006), pp. 516–533.
12. W. E, J. Guo-Liu , *Projection Method I: Convergence and Numerical Boundary Layers*, SIAM J. Numer. Anal., 32 (1995), pp. 1017–1057.
13. W. M, Elsasser, *The Hydromagnetic Equations*, Phy. Rev., 79 (1950), pp. 183–183.
14. M. Farge , *Wavelet transforms and their applications to turbulence*, Ann. Review of Fluid Mechanics., 24(1992), pp. 395-457.
15. M. Farge, N. Kevlahan, V. Perrier, E. Goirand, *Wavelets and Turbulence*, Proceedings of the IEEE, 84 (1996), pp. 639–669.
16. J. Frohlich, K. Schneider, *Numerical Simulation of Decaying Turbulence in an Adaptive Wavelet Basis*, Appl. Comput. Harm. Anal., 3 (1996), pp. 393–397.
17. V. Girault, P.A. Raviart, *Finite element methods for Navier-Stokes equations*, Springer-Verlag Berlin, (1986).
18. S. Grivet-Talocia, A. Tabacco, *Wavelets on the interval with optimal localization*, Math. Models. Meth. Appl. Sci., 10 (2000), pp. 441–462.
19. M. Henry, E. Maitre, V. Perrier ,*Optimal Transport using HelmHoltz-Hodge decomposition and first order Primal-Dual Algorithm*, IEEE ICIP, (2015), pp. 4748–4752.
20. A. Jouini, P.G. Lemarié-Rieusset, *Analyse multirésolution biorthogonale sur l'intervalle et applications*, Annales de l'I.H.P. Section C, 10 (1993), pp. 453–476.
21. S. Kadri-Harouna, V. Perrier, *Helmholtz-Hodge Decomposition on* $[0, 1]^d$ *by Divergence-free and Curl-free Wavelets*, Curves and Surfaces, proc of the 7th International Conference, Avignon, France, June 24-30, 2010, Boissonnat, J.-D.; Chenin, P.; Cohen, A.; Gout, C.; Lyche, T.; Mazure, M.-L.; Schumaker, L. (Eds.), Lecture Notes in Computer Science series, 6920, Springer (2012), pp. 311–329.
22. S. Kadri-Harouna, V. Perrier, *Effective construction of divergence-free wavelets on the square*, J. of Computational and Applied Math, 240 (2013), pp. 74–86.
23. S. Kadri-Harouna, V. Perrier, *Divergence-free wavelet projection method for incompressible viscous flow on the square*, SIAM Multiscale Modeling and Simulation, 13 (2015), pp. 399–422.
24. S. Kadri-Harouna, V. Perrier, *Homogeneous Dirichlet wavelets on the interval diagonalizing the derivative operator, and related applications*, preprint hal-01568431v2, (2018).
25. J. Kim, P. Moin, *Application of a fractional-step method to incompressible Navier-Stokes equations*, J. Comp. Phys., 59 (1985), pp. 308–323.
26. P. G. Lemarié-Rieusset, *Analyses multi-résolutions non orthogonales, commutation entre projecteurs et dérivation et ondelettes vecteurs à divergence nulle*, Revista Matemática Iberoamericana, 8 (1992), pp. 221–236.
27. J.-G. Liu, J. Liu, R. Pego, *Stable and accurate pressure approximation for unsteady incompressible viscous flow*, J. Comput. Phys., 229 (2010), pp. 3428–3453.
28. R. Masson, *Biorthogonal spline wavelets on the interval for the resolution of boundary problems*, M3AS, 6 (1996), pp. 749–791.
29. P. Monasse, V. Perrier, *Orthogonal Wavelet Bases Adapted For Partial Differential Equations With Boundary Conditions*, SIAM J. Math. Anal., 29 (1998), pp. 1040–1065.
30. M. Sass-Hansen, R. Larsen, N.-V. Christensen, *Curl-gradient Image Warping-Introducing Deformation Potentials for Medical Image Registration using Helmholtz Decomposition*, VISSAPP, 1(2009) pp. 79–185.
31. K. Schneider, O. Vasilyev, *Wavelet methods in computational fluid dynamics*, Annu. Rev. Fluid Mech., 42 (2010), pp. 473–503.
32. R. Stevenson, *Divergence-free wavelet bases on the hypercube: Free-slip boundary conditions, and applications for solving the instationary Stokes equations*, Math. Comp. 80 (2011), ppn.1499–1523.
33. R. Stevenson, *Divergence-free wavelets on the hypercube: General boundary conditions*, Constr. Approx., 44 (2016), pp. 233–267.

34. R. Temam, *Sur l'approximation de la solution des équations de Navier-Stokes par la méthode des pas fractionnaires II* , Arch. Rational Mech. Anal. 33 (1969), pp. 377–385.
35. R. Temam, *Navier Stokes Equations, North Holland*, New York, (1977).
36. K. Urban, *Using divergence-free wavelets for the numerical solution of the Stokes problem*, AMLI'96: Proceedings of the Conference on Algebraic Multilevel Iteration Methods with Applications University of Nijmegen, The Netherlands, 2 (1996), pp. 261–277.
37. K. Urban, *Wavelet Bases in $H(div)$ and $H(curl)$*, Math. Comput., 70 (2000), pp. 739–766.
38. C. Wang, J-G. Liu, *Convergence of Gauge method for incompressible flow*, Math. Comput., 69 (2000), pp. 1385–1407.